Distance Dependence and Spatial Distribution of the Molecular Quadrupole Moments of H_2, N_2, O_2, and F_2

D. B. Lawson and J. F. Harrison*

Department of Chemistry and Center for Fundamental Materials Research, Michigan State University, East Lansing, Michigan 48824-1322

Received: January 28, 1997; In Final Form: April 23, 1997[⊗]

We have estimated the complete basis set limits for the Hartree−Fock, MP2, CASSCF, and CASSCF+1+2 wave functions for the titled molecules and calculated the molecular quadrupole moment as a function of bond length. Our recommended values for Θ (v=0,J=0) compare favorably to the current experimental values and previous high-level calculations. To aid in the analysis of the relationship between the molecule's electronic structure and quadrupole moment, we introduce the concept of a quadrupole moment density that permits one to write the molecular quadrupole moment as a sum of the separated atoms quadrupole moments and a purely molecular contribution. The quadrupole density provides a (reference state dependent) means of determining the contribution to Θ from various regions in the molecule and gives considerable insight into the relationship between the electron density and the magnitude and sign of Θ, and it allows a detailed assessment of the contribution of electron correlation to Θ.

Introduction

In this report, we discuss the calculation and interpretation of the quadrupole moments of H_2, N_2, O_2, and F_2. Our primary interest is in developing a qualitative understanding of the relationship between a molecule's quadrupole moment and electronic structure, and, in order to do so reliably, we have explored the sensitivity of the calculated quadrupole moment to basis sets as well as electron correlation. Using SCF, MCSCF, MP2 perturbation theory and multireference configuration interaction, we calculate quadrupole moments, as a function of internuclear separation, for a sequence of basis sets obtained from the Dunning[1a,1b] augmented correlation consistent sets by deleting g and higher symmetries.

We first discuss the quadrupole moments at the calculated equilibrium separations and compare these with experiment and previous calculations. Then, we examine the quadrupole moment functions (variation of the quadrupole moment with the internuclear separation), using MCSCF and MRCI techniques. Finally, we develop an interpretation of the molecular quadrupole moment as the sum of atomic contributions associated with the free (noninteracting) atoms and a molecular contribution that depends on the shift in the electron density due to molecule formation (the deformation density). Using the deformation density, we define a quadrupole density whose integral is the molecular contribution to the molecular quadrupole moment. The distance dependence of the quadrupole moment, the differing contributions to Θ from various regions of the charge distribution, and the role of electron correlation in determining Θ are analyzed in terms of the quadrupole density.

Computational Techniques

Following Dunning,[1] the augmented correlation consistent basis sets are referred to as aug-cc-pv*X*z, where *X* is a cardinal number (2−5) characterizing the basis. Because of technical limitations in the COLUMBUS properties program, we deleted angular functions of g or greater. The SCF, Möller−Plesset, and CISD calculations were done using g92/DFT,[2] while the MCSCF and MRCI calculations used the COLUMBUS[3] system of codes. We use the traceless form of the quadrupole-moment operator,[4] which, for a homonuclear diatomic, reads

$$\hat{\Theta}_{zz} \equiv \hat{\Theta} = -\frac{1}{2}\sum_{i=1}^{N_e}(3z_i^2 - r_i^2) + \frac{1}{2}ZR^2 \qquad (1)$$

where Z is the atomic number of the nuclei in the diatomic and R is the internuclear separation. We use atomic units throughout, except where explicitly noted. In these units, 1 au of quadrupole moment (ea_2^0) contains 1.344 911 B, 4.4866 × 10^{-40} cm^2, and 1.344 911 × 10^{-26} esu cm^2.

We estimate the complete basis set (CBS)[5] limit of a property by fitting the property values to a function of the form

$$P(X) = P(\infty) + Be^{-CX} \qquad (2)$$

where X is the cardinal number of the basis set and $P(X)$ is the property calculated with that basis.

Tables 1−4 collect the quadrupole moments of the titled molecules for various wave functions as a function of basis set. The MP2 wave functions include excitations from the $1\sigma_g$ and $1\sigma_u$ orbitals of N_2, O_2, and F_2. The MCSCF wave functions are CASSCF functions over the MO's derived from the valence p orbitals (the $3\sigma_g$, $3\sigma_u$, $1\pi_{ux}$, $1\pi_{uy}$, $1\pi_{gx}$, $1\pi_{gy}$). The MRCI incorporates all single and double excitations from these six orbitals, as well as all double excitations from the $2\sigma_g$ and $2\sigma_u$ orbitals. The CASSCF wave functions include all valence electrons and the eight orbitals described above, and the CASSCF+1+2 wave function consists of all single and double excitations from the CASSCF reference space. For O_2, both ROHF and UHF results are reported. The quadrupole moments of the SCF, MCSCF, MP2, and CI wave functions were calculated using expectation values. We also computed the MP2 quadrupole moments using energy derivatives, and they differ by ∼1% from the expectation values.

Discussion

Let us look, first, at the H_2 quadrupole data in Table 1. Several characteristics are evident. First, the convergence to

[⊗] Abstract published in *Advance ACS Abstracts,* June 1, 1997.

S1089-5639(97)00342-3 CCC: $14.00

TABLE 1: Calculated and Experimental Constants for the Ground State, X $^1\Sigma_g^+$, of H_2

method basis	r_e (a_0)	E_T (e^2/a_0)	D_e (ev)	ω_e (cm^{-1})	Θ_{zz} (ea_0^2)
RHF					
aug-cc-pvdz	1.4137	−1.128 826	3.5066	4558	0.4613
aug-cc-pvtz	1.3880	−1.133 056	3.6207	4585	0.4916
aug-cc-pvqz	1.3865	−1.133 508	3.6330	4582	0.4867
aug-cc-pv5z	1.3863	−1.133 648	3.6368	4583	0.4852
CBS limit	1.3863	−1.133 6	3.6355		0.4845
MP2					
aug-cc-pvdz	1.4271	−1.156 216	4.2509	4459	0.4401
aug-cc-pvtz	1.3933	−1.165 023	4.4906	4519	0.4719
aug-cc-pvqz	1.3912	−1.166 740	4.5373	4517	0.4679
aug-cc-pv5z	1.3902	−1.167 191	4.5496	4521	0.4662
CBS limit	1.3893	−1.167 3	4.5498		0.4649
CASSCF					
aug-cc-pvqz	1.4047	−1.171 718	4.6728	4382	0.4573
CISD					
aug-cc-pvdz	1.4392	−1.164 900	4.4873	4345	0.4275
aug-cc-pvtz	1.4041	−1.172 636	4.6978	4401	0.4616
aug-cc-pvqz	1.4022	−1.173 867	4.7313	4400	0.4585
aug-cc-pv5z	1.4014	−1.174 175	4.7397	4404	0.4569
CBS limit	1.4010	−1.174 2	4.7403		0.4552
exptl	1.4011[12]		4.7487[12]	4404.7[12]	0.460 ±0.021[10]

TABLE 2: Calculated and Experimental Constants for the Ground State, X $^1\Sigma_g^+$, of N_2

method basis	r_e (a_0)	E_T (e^2/a_0)	D_e (ev)	ω_e (cm^{-1})	Θ_{zz} (ea_0^2)
RHF					
aug-cc-pvdz	2.0377	−108.961 925	4.9576	2736	−0.9490
aug-cc-pvtz	2.0163	−108.987 796	5.2404	2726	−1.0090
aug-cc-pvqz	2.0135	−108.994 616	5.2836	2730	−1.0118
aug-cc-pv5z	2.0133	−108.995 999	5.2870	2729	−1.0149
CBS limit	2.0133		5.2891		−1.0158
MP2					
aug-cc-pvd	2.1388	−109.280 650	9.4100	2157	−1.1262
aug-cc-pvtz	2.1053	−109.364 800	10.0293	2187	−1.1626
aug-cc-pvqz	2.0985	−109.383 055	10.1363	2200	−1.1710
aug-cc-pv5z	2.0976	−109.388 586	10.1731	2206	−1.1747
CBS limit	2.0970		10.1724		−1.1751
MCSCF					
aug-cc-pvdz	2.1076	−109.097 018	8.6337	2351	−1.1683
aug-cc-pvtz	2.0853	−109.120 694	8.8568	2348	−1.2260
aug-cc-pvqz	2.0825	−109.127 412	8.8973	2352	−1.2292
CBS limit	2.0821		8.9063		−1.2294
CASSCF					
aug-cc-pvqz	2.0860	−109.139 872	9.2364	2340	−1.1753
MRCI					
aug-cc-pvdz	2.1144	−109.284 004	8.7673	2328	−1.1079
aug-cc-pvtz	2.0866	−109.367 229	9.5037	2335	−1.1390
aug-cc-pvqz	2.0806	−109.383 822	9.5698	2344	−1.1464
CBS limit	2.0789		9.5721		−1.1487
CASSCF+1+2					
aug-cc-pvqz	2.0827	−109.386 811	9.5755	2337	−1.1247
"CBS limit"	2.0810				−1.1270
exptl	2.0744[12]		9.9065[12]	2358.6[12]	−1.09 ± 0.07[36]

the CBS limit is only monotonic after the aug-cc-pvdz basis, and accordingly, we use the last three basis sets to extrapolate to the CBS limit. Within these three basis sets, increasing the flexibility of the basis decreases Θ, as does increasing the level of correlation. The aug-cc-pv5z basis set results are close to the CBS limit for each model wave function.

Note that the CBS-CISD limit predicts an equilibrium bond length $R_{opt} = 1.4010a_0$ and a dissociation energy $D_e =$ 4.740 ev, in excellent agreement with the experimental values[12] $1.4011a_0$ and 4.749 ev. Our CBS-CISD value of Θ is $+0.455ea_0^2$ and agrees with the essentially exact theoretical result[8] of $+ 0.457ea_0^2$. The experimental value for Θ, $+0.460 \pm 0.021ea_0^2$, is an indirect value assembled from the magnetic susceptibility anisotropy and the molecular g value, assuming a vibrationless H_2.[7−9] As such, it agrees well with our CBS-CISD estimate of the vibrationless Θ, $+0.455ea_0^2$. Buckingham and Cordle[10] have estimated the vibrational ($v = 0, J = 1$) value to be $0.4853ea_0^2$. Figure 2 shows the variation of Θ with R for the SCF and CISD wave functions, using the aug-cc-pvqz basis. These data were fit to a quadratic function of the form

$$\Theta(R) = \Theta(R_{opt}) + \left(\frac{d\Theta}{dR}\right)_{opt}(R - R_{opt}) + \left(\frac{d^2\Theta}{dR^2}\right)_{opt}\frac{(R - R_{opt})^2}{2} \quad (3)$$

and the parameters are reported in Table 5. These data are useful in correcting our calculated values to other bond lengths for comparison with previous calculations. Additionally, they allow us to estimate the vibrational dependence of Θ, using the formula[10,11]

$$\Theta_v = \Theta_{opt} + \frac{B_e}{\omega_e}\left[3\left(1 + \frac{\alpha_e\omega_e}{6B_e^2}\right)R_{opt}\left(\frac{d\Theta}{dR}\right)_{R_{opt}} + R_{opt}^2\left(\frac{d^2\Theta}{dR^2}\right)_{R_{opt}}\right](v + {}^1/_2) \quad (4)$$

and experimental values[12] for the spectroscopic parameters α_e,

TABLE 3: Calculated and Experimental Constants for the Ground State, X $^3\Sigma_g^-$, of O_2

method basis	r_e (a_0)	E_T (e^2/a_0)	D_e (ev)	ω_e (cm^{-1})	Θ_{zz} (ea_0^2)
RoHF					
aug-cc-pvdz	2.1840	−149.625 220	1.1784	2018	−0.2833
aug-cc-pvtz	2.1779	−149.660 506	1.2923	2001	−0.3928
aug-cc-pvqz	2.1749	−149.670 308	1.3110	2006	−0.4085
aug-cc-pv5z	2.1747	−149.672 974	1.3186	2008	−0.4183
CBS limit	2.1739		1.3181		−0.4188
UHF					
aug-cc-pvdz	2.1979	−149.646 215	1.7497	2025	−0.2341
aug-cc-pvtz	2.1915	−149.682 470	1.8899	1960	−0.3134
aug-cc-pvqz	2.1885	−149.692 404	1.9124	1965	−0.3273
aug-cc-pv5z	2.1885	−149.695 099	1.9207	1966	−0.3356
CBS limit	2.1889		1.9172		−0.3427
UMP2					
aug-cc-pvdz	2.3314	−150.011 480	5.2852	1428	−0.1107
aug-cc-pvtz	2.3138	−150.128 401	5.6078	1455	−0.2178
aug-cc-pvqz	2.3064	−150.153 761	5.6322	1467	−0.2421
aug-cc-pv5z	2.3049	−150.162 153	5.6548	1465	−0.2537
CBS limit	2.3032		5.6472		−0.2546
MCSCF					
aug-cc-pvdz	2.3022	−149.718 078	3.7982	1550	−0.1457
aug-cc-pvtz	2.2975	−149.752 814	3.9146	1543	−0.2618
aug-cc-pvqz	2.2939	−149.763 505	3.9606	1548	−0.2858
CBS limit	2.2936		3.9906		−0.2920
CASSCF					
aug-cc-pvqz	2.2973	−149.768 890	4.1072	1544	−0.2822
MRCI					
aug-cc-pvdz	2.3072	−150.003 808	4.4229	1551	−0.1213
aug-cc-pvtz	2.2921	−150.114 527	4.9575	1565	−0.2156
aug-cc-pvqz	2.2864	−150.138 411	5.0034	1495	−0.2474
CBS limit	2.2830		5.0077		−0.2636
CASSCF+1+2					
aug-cc-pvqz	2.2907	−150.140 112	5.0056	1564	−0.2368
exptl	2.2818[12]		5.2318[12]	1580.2[12]	-0.3 ± 0.1[41]

TABLE 4: Calculated and Experimental Constants for the Ground State, X $^1\Sigma_g^+$, of F_2

method basis	r_e (a_0)	E_T (e^2/a_0)	D_e (ev)	ω_e (cm^{-1})	Θ_{zz} (ea_0^2)
RHF					
aug-cc-pvdz	2.5288	−198.703 251	1.3847	1216	0.5229
aug-cc-pvtz	2.5099	−198.760 936	1.1764	1271	0.3558
aug-cc-pvqz	2.5090	−198.774 915	1.1770	1264	0.3321
aug-cc-pv5z	2.5071	−198.779 081	1.1786	1267	0.3149
CBS limit	2.5079	−198.780 1	1.1792		0.3180
MP2					
aug-cc-pvdz	2.6959	−199.126 917	1.5039	934	0.9254
aug-cc-pvtz	2.6490	−199.290 907	1.7987	1002	0.7588
aug-cc-pvqz	2.6471	−199.326 593	1.7931	1013	0.7374
aug-cc-pv5z	2.6452	−199.338 340	1.8004	1017	0.7199
CBS limit	2.6460	−199.339 9	1.7970		0.7236
MCSCF					
aug-cc-pvdz	2.8257	−198.777 612	0.6388	637	0.9873
aug-cc-pvtz	2.7643	−198.832 379	0.7677	718	0.7899
aug-cc-pvqz	2.7632	−198.846 561	0.7658	731	0.7651
CBS limit	2.7632	−198.851 5	0.7681		0.7616
CASSCF					
aug-cc-pvqz	2.7598	−198.848 763	0.8257	731	0.7611
MRCI					
aug-cc-pvdz	2.7520	−199.119 575	1.2603	791	0.9370
aug-cc-pvtz	2.6838	−199.277 054	1.4875	889	0.7356
aug-cc-pvqz	2.6825	−199.310 003	1.4879	886	0.7111
CBS limit	2.6827	−199.318 7	1.4906		0.7077
CASSCF+1+2					
aug-cc-pvqz	2.6853	−199.311 6	1.5021	887	0.7165
exptl	2.6681[12]		1.6916[12]	916.6[12]	1.0−1.3[33]
					0.56[34]

ω_e, and B_e. Using eq 3 and our R_{opt} for the HF and CISD wave functions, we corrected Θ to the experimental $R_{exptl} = 1.4011$ a_0 at which most other calculations were done. Our HF result at R_{exptl} is $0.4937ea_0^2$, in excellent agreement with the numerical HF result ($0.4934ea_0^2$) of Laaksonen, Pyykkö, and Sundholm.[13] Using eq 4 and the data in Table 5, we estimate the vibrational dependent CBS-CISD value of Θ to be

$$\Theta(H_2;v) = +0.455 + 0.051(v + {}^1/_2)$$

$$\text{or } \Theta(H_2;v{=}0) = 0.481ea_0^2$$

which is in good agreement with the $v = 0$, $J = 0$ values of Wolniewicz,[14] $0.484ea_0^2$ and Kosmasa and Thakhar,[15] $0.483ea_0^2$, and the $v = 0$, $J = 1$ value, $0.4853ea_0^2$, of Buckingham and Cordle.[10] There are a vast number of calculations[6−8,13−19] of $\Theta(H_2)$, and we collect, in Table 6, a representative collection of *ab-initio* values for $\Theta(H_2)$, along with the experimental values and our CBS-HF and CBS-CISD results.

From Table 5, we see that the slope of $\Theta(H_2)$ around R_{opt} is positive, as it is for N_2, O_2, and F_2. Accordingly, to the extent that the RHF model limit for R_{opt} is less than R_{exptl}, the HF

TABLE 5: Equilibrium Value of the First and Second Derivatives of the Molecular Quadrupole Moment Function for H_2, N_2, O_2, and F_2, Calculated with Various Wave Functions

molecule	wave function	R_{opt} (a_0)	$(d\Theta/dR)_{R_{opt}}$ (ea_0)	$(d^2\Theta/dR^2)_{R_{opt}}$ (e)
H_2	SCF	1.3865	0.6064	0.2622
H_2	CISD	1.4022	0.5174	0.1028
N_2	SCF	2.0133	1.4017	0.5594
N_2	MCSCF	2.0825	0.9481	0.0548
N_2	MRCI	2.0806	0.9593	0.0892
O_2	ROSCF	2.1747	1.4797	−0.0744
O_2	MCSCF	2.2939	1.3720	−0.1998
O_2	MRCI	2.2864	1.4738	−0.2160
F_2	SCF	2.5071	1.1656	−0.6212
F_2	MCSCF	2.7632	1.1399	−0.9718
F_2	MRCI	2.6825	1.2134	−0.9142

model limit for Θ is always less than the HF value calculated at R_{exptl}. Note that electron correlation decreases Θ relative to the HF value. Precisely how much depends on whether one compares the HF and correlated value at the experimental bond length or at the optimal bond length (R_{opt}) corresponding to each model. Since correlation corrections to the HF wave function are responsible for changing the predicted R_{opt}, measuring correlation effects relative to the experimental bond length obscures this important effect. For example, Θ(CISD) at the experimental bond length is 7.8% smaller than Θ(HF) at this bond length, while Θ(CISD) and Θ(HF) differ by 6.0% when each is referred to its model limit R_{opt}.

Our N_2 results are summarized in Table 2 and compared with selected calculations[18,21−32] and experiments[36,37] in Table 7. As with H_2, increasing the quality of the basis set within a model reduces the calculated Θ and adding correlation decreases Θ, relative to the SCF values. Our CBS-HF limit is $-1.0158ea_0^2$ at R_{opt} of $2.0133a_0$ and $-0.9306ea_0^2$ at $R = 2.074\,32a_0$, in excellent agreement with the numerical HF result[20] of $-0.9310ea_0^2$ at this bond length. The convergence of the MP2, MCSCF, and MRCI results all suggest that the aug-cc-pvqz basis produces a quadrupole moment that differs

TABLE 6: Section of H_2 Quadrupole Moments

R (a_0)	Θ (ea_0^2)	ref	comment
1.4	0.493	17	Hartree−Fock limit
1.4	0.493422	13	numerical HF
1.405	0.4898	15	SCF, derivative Hartree−Fock, ELP basis
1.3863	0.4845	LH[a]	CBS-HF; R_{opt}
1.4016	0.4937	LH[a]	CBS-HF; exptl R_e
1.4	0.457	6	essentially exact wave function
1.401	0.437	18	numerical DFT
1.40	0.4438	19	MP4 Sadlej[16] basis
1.40	0.4414	19	CISD Sadlej basis
1.405	0.4512	15	CISD, ELP basis
1.40	0.456444	15	explicitly correlated Gaussian, essentially exact wave function
1.3895	0.4649	LH[a]	CBS-MP2 R_{opt}
1.4016	0.4712	LH[a]	CBS-MP2 exptl R_e
1.4010	0.4552	LH[a]	CBS-CISD R_{opt}
vibrational average	0.516	LH[a]	CBS-HF; $v = 0$, $J = 0$
vibrational average	0.481	LH[a]	CBS-CISD; $v = 0$, $J = 0$
vibrational average	0.477	20	integrate radial wave function
vibrational average	0.483103	15	explicitly correlated Gaussian, essentially exact wave function, integrate radial wave function, $v = 0$, $J = 0$
exptl	0.470 ± 0.021	8	derived from exptl data—nonvibrating molecule
exptl	0.485	10	vibrational average of magnetic anisotropy and g factor; $v = 0$, $J = 1$

[a] This work.

TABLE 7: Selection of N_2 Quadrupole Moments

R (a_0)	Θ (ea_0^2)	ref	comment
2.07432	−0.9310	2	numerical HF
2.068	−0.9400	22, 23	numerical HF
2.07432	−0.9054	24	SCF large basis
2.07430	−0.9285	25	SCF large basis
2.068	−0.937	26	SCF
2.105	−0.8858	31	derivative Hartree−Fock, ELP basis
2.0133	−1.0158	LH[a]	SCF at R_{opt}
2.07435	−0.9306	LH[a]	CBS-SCF limit
2.075	−1.137	18	numerical DFT
2.068	−1.1426	27	numerical HFS
2.07430	−1.1289	28	large basis set DFT
2.068	−1.15	29	numerical HFS
2.07432	−1.1131	24	SDQ-MPPT(4); 6s4p3d1f
2.07430	−1.0905	25	MRSD-CI
2.068	−1.154	26	MRSD-CI
2.068	−1.16865	30	CCSD-Sadlej's[16] 5s4p2d basis
2.105	−1.0846	31	AACD-ELP basis
2.0856	−1.1755	LH[a]	CBS-CASSCF; R_{opt}
2.0810	−1.1270	LH[a]	CBS-CASSCF+1+2; R_{opt}
2.07432	−1.1334	LH[a]	CBS-CASSCF+1+2; R_{exptl}
vibrational average	−1.118	LH[a]	CBS-CASSCF+1+2; $v = 0$, $J = 0$
vibrational average	−1.1557	35	CCSD, $v = 0$, $J = 0$; Sadlej's 5s4p2d basis
exptl	−1.09 ± 0.07	36	optical birefringence
exptl	−1.05 ± 0.06	37	optical birefringence

[a] This work.

TABLE 8: Comparison of Experimental and Theoretical Quadrupole-Moment Derivatives for N_2

$(d\Theta/dR)_{R_e}$ (ea_0)	ref	comment
+0.94	43	quadrupole absorption
+0.97	44	collision-induced
+0.95	45	collision-induced
+0.933 ± 0.039	46	quadrupole absorption
0.959	LH[a]	MRCI aug-cc-pvqz; R_{opt}
0.948	LH[a]	MCSCF aug-cc-pvqz; R_{opt}
1.402	LH[a]	SCF aug-cc-pvqz; R_{opt}

[a] This work.

from the CBS limit by less than 0.2%, suggesting that the individual CASSCF and CASSCF+1+2 values of $-1.1753ea_0^2$ and $-1.1247ea_0^2$ are near the model limit. From Table 5, we see the similarity between the MCSCF and the MRCI Θ versus R curves around R_{opt}. The SCF curve has significantly larger first and second derivatives, and these are in good agreement with calculations by Truhlar[38] and Maroulis and Bishop.[39] Using the MRCI derivatives in Table 5, we estimate the vibrational dependence of the CBS-CASSCF+1+2 quadrupole moment as

$$\Theta(N_2;v) = -1.1247 + 0.0137(v + {}^1/_2)$$

and so our recommended vibrationally corrected quadrupole moment is $\Theta(N_2;v{=}0) = -1.118ea_0^2$. This is in good agreement with the reported experimental quadrupole moments gathered in Table 7. The several experimental estimates of the quadrupole derivative available in the literature[43−46] average $0.95ea_0$, and these may be compared with our SCF, MCSCF, and MRCI results of $1.402ea_0$, $0.948ea_0$, and $0.959ea_0$. The SCF result is clearly much too large, while the correlated values agree with the average of the experimental values. The data are collected in Table 8. Note that the significant reduction in $d\Theta/dR$, when a correlated wave function is used, is implicit in the SCF vs GVB results reported by Cartwright and Dunning.[40]

Our O_2 results are summarized in Table 3. As with H_2 and N_2, increasing the quality of the basis set decreases the quadrupole moment. However, unlike H_2 and N_2, adding correlation increases the quadrupole moment (makes it less negative). The opposing effects of basis-set quality and correlation permits a limited correlation wave function with a small basis set to predict a quadrupole moment comparable with the CBS-MRCI limit. We have not found a reported Hartree−Fock limit for $\Theta(O_2)$ with which to compare either our ROHF results ($R_{opt} = 2.1747a_0$, $\Theta = -0.1488ea_0^2$) or our UHF results ($R_{opt} = 2.1885a_0$, $\Theta = -0.3427ea_0^2$). Our ROHF and UHF results at $R = 2.28a_0$ are $-0.264ea_0^2$ and $-0.218ea_0^2$, respectively and are in reasonable agreement with a large basis SCF calculation, by Bündgen *et al.*,[26] at $R = 2.2819a_0$ that predicts $\Theta = -0.249\ ea_0^2$. There are two numerical HFS calculations of Θ, both at $R = 2.28\ a_0$. The first, by Becke,[29] is an unrestricted calculation that predicts $\Theta = -0.36\ ea_0^2$, while the second, by Laaksonen *et al.*,[27] is a spin-restricted calculation predicting $\Theta = -0.3885ea_0^2$.

Our CBS CASSCF and CASSCF+1+2 results are $-0.2885ea_0^2$ and $-0.2530ea_0^2$, respectively. It is fascinating that ROHF calculations at the experimental bond length predict a $\Theta(-0.264ea_0^2)$, which differs from our best correlated result ($-0.253ea_0^2$) by only 4%. The reason for the insensitivity of $\Theta(O_2)$ to correlation effects is a consequence of the difference in the response of the σ and π electrons in O_2 to electron correlation and will be discussed after the quadrupole density is introduced. The first and second derivatives of these curves are collected in Table 5.

TABLE 9: Selection of O_2 Quadrupole Moments

R (a_0)	Θ (ea_0^2)	ref	comment
2.1747	−0.4188	LH[a]	ROHF; R_{opt}
2.1885	−0.3427	LH[a]	UHF; R_{opt}
2.28	−0.2634	LH[a]	ROHF
2.28	−0.188	26	SCF Sadlej[16] basis (5s3p2d)
2.28	−0.249	26	SCF
2.2819	−0.271	48	CI
2.282	−0.356	18	numerical DFT (unrestricted)
2.28	−0.3885	27	numerical HFS ($\alpha = 0.7$)
2.28	−0.36	29	numerical HFS (restricted)
2.2970	−0.2885	LH[a]	CBS-CASSCF; R_{opt}
2.2873	−0.2530	LH[a]	CBS-CASSCF+1+2; R_{opt}
vibrational average	−0.240	LH[a]	CBS-CASSCF+1+2
exptl	|0.25|	42, 47	pressure-induced, far-infrared spectrum
exptl	−0.3 ± 0.1	41	optical birefringence

[a] This work.

Experimental data on O_2 is sparse. Buckingham *et al.*[41] report $-0.3 \pm 0.1ea_0^2$ from induced birefringence measurements, and Cohen and Birnbaum[42,47] report $|\Theta| = 0.25ea_0^2$ obtained from the interpretation of pressure-induced far-infrared spectra. These, and selected theoretical results, are shown in Table 9. Using the derivatives in Table 5, we estimate that the vibrational correction to our CBS-CASSCF+1+2 result is

$$\Theta(O_2;v) = -0.2530 + 0.0257(v + {}^1/_2)$$

resulting in $\Theta(O_2,v{=}0) = -0.2273ea_0^2$, which is in general agreement with the highly uncertain experimental values. The experimental estimate[43] of $(d\Theta/dR)_{exptl}$ for O_2, obtained from an analysis of the quadrupole absorption spectrum, is $+1.6ea_0$ and is in reasonable agreement with our ROHF, MCSCF, and MRCI values of 1.8, 1.4, and $1.5ea_0$, respectively.

Our F_2 results are collected in Table 4. As with H_2, N_2, and O_2, the quadrupole moment decreases within a model with increasing quality of basis set and as in O_2, electron correlation increases Θ. Our CBS-RHF limit is $+0.3081ea_0^2$ at $R_{opt} = 2.5064a_0$ and $+0.501ea_0^2$ at $R = 2.68a_0$. This latter value is in good agreement with the numerical Hartree−Fock result of McCullough,[23] $+0.505ea_0^2$, at $R = 2.68a_0$. Our CBS-CASSCF+1+2 value of $+0.7165ea_0^2$ ($R_{opt} = 2.6853a_0$) is in good agreement with the numerical HFS calculations of Laaksonen *et al.*,[27] $0.6911ea_0^2$ at $R = 2.68a_0$, and those of Becke,[29] $+0.69ea_0^2$ also at $R = 2.68a_0$. Our CBS limit at $R = 2.68a_0$ is $+0.7068ea_0^2$. Correlation correction effects more than double $\Theta(F_2)$, a much larger effect than in H_2, N_2, and O_2. This substantial correlation effect is consistent with the results of Dykstra[31] *et al.* and Maroulis and Thakkar.[32] These latter authors report a SCF value of $0.5157ea_0^2$ and a SDQ-MPPT(4) value of $0.7466ea_0^2$, both calculated at $R = 2.66816a_0$. As we will see subsequently, the correlation corrections to Θ, due to the σ and π electrons, are both in the same direction, and, rather than cancel as in O_2, they reinforce one another. Using the data in Table 4, we write the vibrational averaged Θ as

$$\Theta(F_2;v) = +0.7131 + 0.0276(v + {}^1/_2)$$

and, so, $\Theta(F_2;0) = +0.7269ea_0^2$. We collect the values of Θ from selected calculations in Table 10. The experimental measurements[33,34] of $\Theta(F_2)$, $1.0-1.3ea_0^2$ and $0.56ea_0^2$ have large uncertainties associated with them. We have collected the CASSCF+1+2 values of Θ along with the estimated CBS limit and vibrational corrections in Table 11.

MP2 Results

It is apparent, from Tables 1−4, that MP2 is a significant improvement over the SCF model with little additional effort.

TABLE 10: F_2 Quadrupole Moments

R (a_0)	Θ (ea_0^2)	ref	comment
2.68	0.505	23	numerical HF
2.6681	0.5447	31	derivative Hartree−Fock, ELP basis
2.68	0.659	49	SCF
2.66816	0.7466	32	SDQ-MPPT(4) 6s5p3d1f basis
2.66816	0.5157	32	SCF 6s5p3d1f basis
2.5064	0.3081	LH[a]	CBS-HF; R_{opt}
2.68	0.501	LH[a]	CBS-HF; R_{exptl}
2.68	0.6911	27	numerical HFS ($\alpha = 0.7$)
2.68	0.69	29	numerical HFS ($\alpha = 0.7$)
2.6681	0.6880	31	ACCD, ELP basis
2.6853	0.7131	LH[a]	CBS-CASSCF+1+2; R_{opt}
2.68	0.707	LH[a]	CBS-CASSCF+1+2; R_{eq}
vibrational average	0.727	LH[a]	CBS-CASSCF+1+2; $v = 0$ $J = 0$
exptl	1.0−1.3	33	fitting of pressure second virial coefficients
exptl	0.56	34	fitting of pressure and dielectric second virial coefficients

[a] This work.

We collect our MP2 results in Table 11 and compare them to the corresponding CBS CASSCF+1+2 results. The comparison is striking and suggests strongly that the corrections due to MP3 and MP4 cancel one another significantly. This has been seen by Wolinski *et al.*[16] and Maroulis and Thakkar[24] and is being further investigated in this laboratory.[50]

Quadrupole Moment Functions

We study the distance dependence of Θ (quadrupole-moment function), using the aug-cc-pvqz basis and the MCSCF and MRCI wave functions. These wave functions provide a reasonably accurate description of the molecule's electronic structure over a large range of internuclear distances, and we expect the calculated quadrupole-moment functions to be realistic.

The quadrupole moment functions for the four molecules of interest are shown in Figure 1, from which we see that H_2 is unique—having the only quadrupole-moment function that is everywhere positive. Θ for H_2 and N_2 is zero at large R because both molecules separate to atoms in S states. Θ for F_2 and O_2 separates to the sum of the atomic quadrupole moments of the atoms. For F_2, the F atoms are in the $^2P_{m=0}$ (^2P_z) state, loosely corresponding to the configuration

$$1s^2 2s^2 2p_x^2 2p_y^2 2p_z^1$$

with z labeling the internuclear axis. For O_2, the atoms are in the $^3P_{|M|=1}$ levels, which, in a real representation, corresponds to one atom in

$$1s^2 2s^2 2p_x^2 p_y^1 p_z^1$$

and one in

$$1s^2 2s^2 2p_x^1 2p_y^2 2p_z^1$$

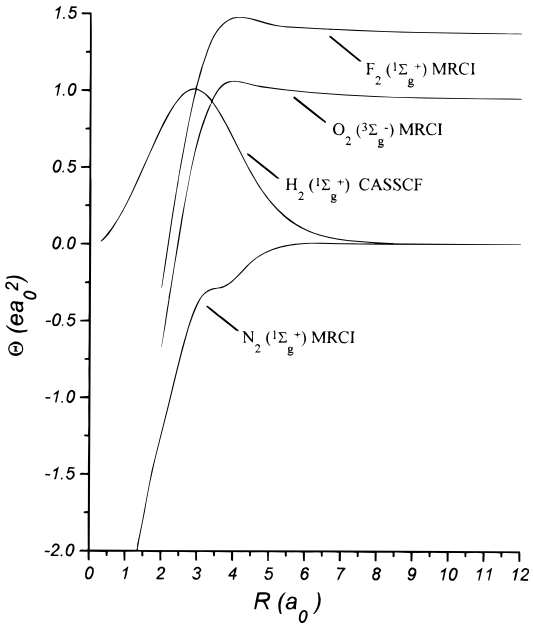

Figure 1. Molecular quadrupole moments of H_2, N_2, O_2, and F_2 as a function of bond length.

We will first consider N_2, O_2, and F_2, returning to H_2 latter. Let us first write the electron density at internuclear separation R as

$$n(\vec{r};R) = n_A^0(\vec{r}) + n_B^0(\vec{r}) + \delta n(\vec{r};R) \tag{5}$$

where n_A^0 and n_B^0 are the electron densities of the two noninteracting atoms placed at the appropriate nuclear positions. Note that δn is defined by this equation. As a practical matter, n_A^0 and n_B^0 are obtained from the natural orbitals of the MCSCF or MRCI wave functions at large values of R and translated, intact, to the internuclear separation of interest.

Using eq 5, the quadrupole moment defined by eq 1 can be rewritten as

$$\Theta(A_2;R) = 2\Theta^0(A) + \int \delta\Theta(\vec{r};R)\, dV \tag{6}$$

where $\Theta^0(A)$ is the quadrupole moment of the separated atom A in the diatomic A_2

$$\Theta^0(A) = -\frac{1}{2}\int n_A^0(\vec{r})(3z^2 - r^2)\, dV \tag{7}$$

and $\delta\Theta$ is the quadrupole-moment density

$$\delta\Theta = -\frac{1}{2}\,\delta n(\vec{r};R)(3z^2 - r^2) \tag{8}$$

Note that the nuclear contribution to $\Theta(A_2;R)$ is now implicit in $\delta n(\vec{r};R)$. Note, also, that $\Theta(A_2;R)$ is now written as the sum of a (constant) atomic contribution, $2\Theta^0(A)$ and a contribution

TABLE 11: Comparison of MP2 and CASSCF+1+2 Results

	aug-cc-pvqz		MP2 (estimated CBS)		CASSCF+1+2 (estimated CBS)		
molecule	R_{opt} (a_0)	Θ (ea_0^2)	R_{opt} (a_0)	Θ (ea_0^2)	R_{opt} (a_0)	Θ (ea_0^2)	vibration correction
H_2	1.4014	+0.4569	1.3895	+0.4699	1.4009	+0.4552	+ 0.051 ($v + 1/2$)
N_2	2.0827	−1.1247	2.0970	−1.1751	2.0810	−1.1270	+0.0137 ($v + 1/2$)
O_2	2.2907	−0.2368	2.3032	−0.2546	2.2873	−0.2530	+0.0257 ($v + 1/2$)
F_2	2.6853	+0.7165	2.6452	+0.7178	2.6853	+0.7131	+0.0276 ($v + 1/2$)

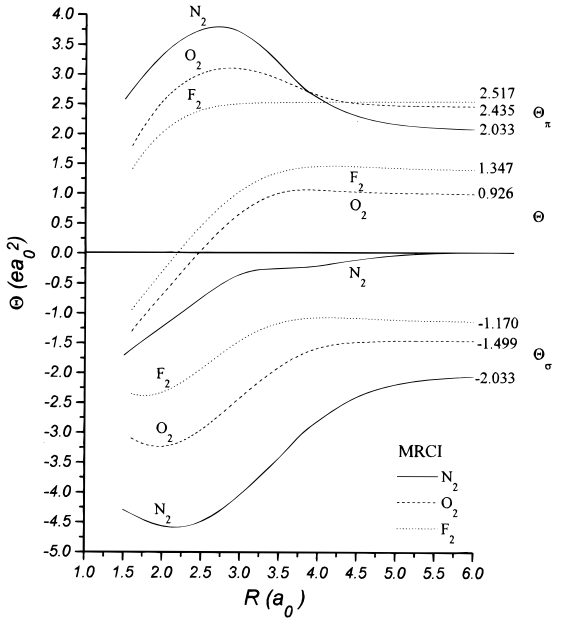

Figure 2. Distance dependence of the molecular quadrupole moments of N_2, O_2, and F_2 partitioned into the Θ_σ and Θ_π components.

Θ_{mol}, due to molecule formation

$$\Theta_{mol}(R) = \int \delta\Theta(\vec{r};R)\, dV \tag{9}$$

Since we may easily partition δn into σ and π contributions

$$\delta n = \delta n_\sigma + \delta n_\pi \tag{10}$$

we may also write

$$\Theta(A_2;R) = \Theta_\sigma(A_2;R) + \Theta_\pi(A_2;R) \tag{11}$$

where

$$\Theta_\sigma(A_2;R) = 2\Theta^0_\sigma(A) + \int \delta\Theta_\sigma(\vec{r};R)\, dV \tag{12}$$

with an analogous expression for $\Theta_\pi(A_2;R)$. The σ and π components of the quadrupole-moment curves for N_2, O_2, and F_2 are shown in Figure 2 for a MRCI wave function in an aug-cc-pvqz basis. Note that Θ_σ is always negative and Θ_π is always positive; while the sign of Θ depends on the relative magnitudes of these contributions, Θ usually decreases from its asymptotic value with decreasing R. The relative asymptotic values are easily understood, in terms of an orbital model. For example, the *zz* component of the atomic quadrupole moment of (oriented, $m = 0$) F is given by

$$\Theta(F;^2P_z) = \Theta(2p_z) + 2\Theta(2p_y) + 2\Theta(2p_x)$$

where

$$\Theta(2p_\alpha) = -\frac{1}{2}\int (2p_\alpha)^2(3z^2 - r^2)\, dV$$

By symmetry

$$\Theta(2p_x) = \Theta(2p_y)$$

and

$$\Theta(2p_x) + \Theta(2p_y) + \Theta(2p_z) = 0$$

With *z* as the internuclear line

$$\Theta_\pi(F) = 2\Theta(2p_x) + 2\Theta(2p_y) = -2\Theta(2p_z) \equiv -2\Theta_\sigma(F)$$

It is easy to show

$$\Theta(2p_z) = \Theta_\sigma(F) < 0$$

so in an orbital model where all 2p orbitals are radially equivalent

$$\Theta_\pi(F) = -2\Theta_\sigma(F) > 0$$

Our asymptotic values are

$$\Theta_\pi(F) = +2.517ea_0^2$$

$$\Theta_\sigma(F) = -1.170ea_0^2$$

These are not precisely in the symmetry-determined ratio because our wave function has D_{2h} symmetry and our correlated wave function results in asymptotic p functions that are not equivalent.

In a similar fashion, the O ($^3P_{|M|=1}$) quadrupole moment is given by

$$\Theta(O;^3P_{|M|=1}) = 2\Theta(2p_x) + \Theta(2p_y) + \Theta(2p_z)$$

$$\Theta_\pi(O) = 2\Theta(2p_x) + \Theta(2p_y)$$

$$\Theta_\sigma(O) = \Theta(2p_z)$$

$$\Theta_\pi(O) = 3\left(-\frac{1}{2}\Theta_\sigma(O)\right) = -{}^3/_2\Theta_\sigma(O)$$

Our asymptotic values are

$$\Theta_\pi(O) = +2.435ea_0^2$$

$$\Theta_\sigma(O) = -1.499ea_0^2$$

They differing from the simple orbital ratios for reasons described earlier.

If we reference each molecular quadrupole-moment function to its asymptotic atomic contribution, we obtain Figures 3−5, which are simply $\Theta_{mol}(R)$ and its component Θ^σ_{mol} and Θ^π_{mol}. Some insight into why Θ^σ_{mol} is always negative and Θ^π_{mol} is always positive may be obtained by examining $\delta\Theta_\sigma(\vec{r};R)$ and $\delta\Theta_\pi(\vec{r};R)$. Recall

$$\delta\Theta_\sigma = -{}^1/_2\delta n_\sigma(\vec{r};R)(3z^2 - r^2) = -{}^1/_2 r^2 \delta n_\sigma(\vec{r};R)(3\cos^2\theta - 1) \tag{13}$$

where the origin is the molecular midpoint and θ is measured relative to the internuclear line as the polar axis. This equation relates electron shifts in the σ system, upon bond formation to the molecular contribution to the quadrupole moment. Note that the factor $-{}^1/_2(3\cos^2\theta - 1)$ partitions the molecular space into two regions, labeled N and P and shown in Figure 6. It is interesting to note that the parabolas delineating the Berlin[52] bonding and antibonding regions are asymptotically tangent to the nodal surfaces separating the N and P regions. In the connical regions labeled N, to the rear of the nuclei, the angular

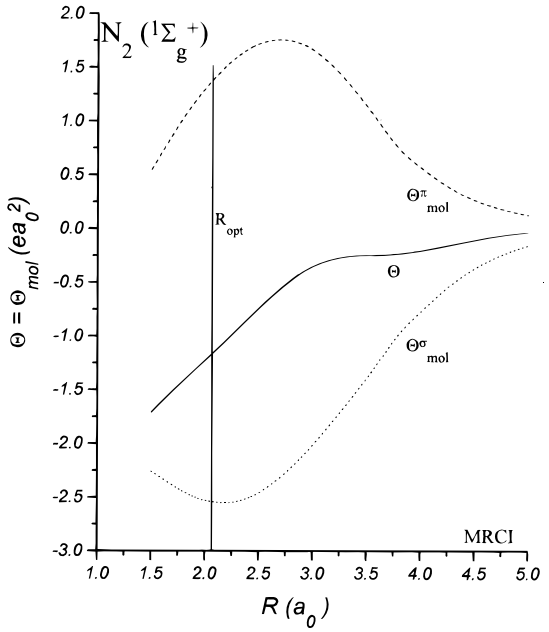

Figure 3. Distance dependence of the quadrupole moment of N_2 partitioned into its Θ^{σ}_{mol} and Θ^{π}_{mol} components.

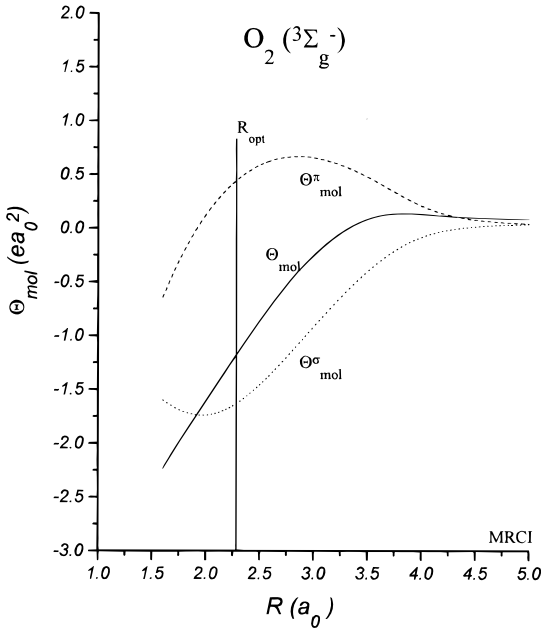

Figure 4. Distance dependence of Θ_{mol} for O_2 partitioned into its Θ^{σ}_{mol} and Θ^{π}_{mol} components.

factor is negative, and thus, a positive δn_σ in this region results in a negative contribution to Θ^{σ}_{mol}. In N_2, the σ bond involves a large sp hybridization, moving charge toward the midpoint of the molecule. Simultaneously, the opposite-phase sp hybrid pooches out to the rear of the nuclei contributing to a positive δn_σ and, therefore, a negative $\delta\Theta_\sigma$. Note that this effect is enhanced by the r^2 term in eq 13, which weights heavily the farther reaches of δn_σ. Along with the σ bond in N_2, we, of course, have the π bond, which results in δn_π being positive in the region between the nuclei and above the molecular line; since $\delta\Theta_\pi = {}^1/_2 r^2 \delta n_\pi (3\cos^2\theta - 1)$, this is precisely where the angular factor is positive, and, therefore, an accumulation of charge in the π system (positive δn_π) results in a positive value of $\delta\Theta_\pi$ and contributes toward a positive value of Θ^{π}_{mol}. These effects are vividly illustrated in Figure 7, which shows δn, δn_σ, and δn_π and the associated $\delta\Theta$, $\delta\Theta_\sigma$, and $\delta\Theta_\pi$ densities for N_2. Note that the increase in charge density around the molecular midpoint contributes little to Θ_{mol}, as it is multiplied

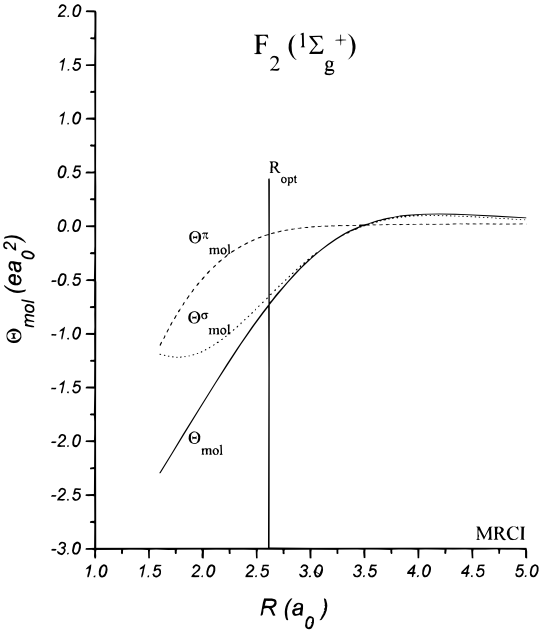

Figure 5. Distance dependence of Θ_{mol} for F_2 partitioned into its Θ^{σ}_{mol} and Θ^{π}_{mol} components.

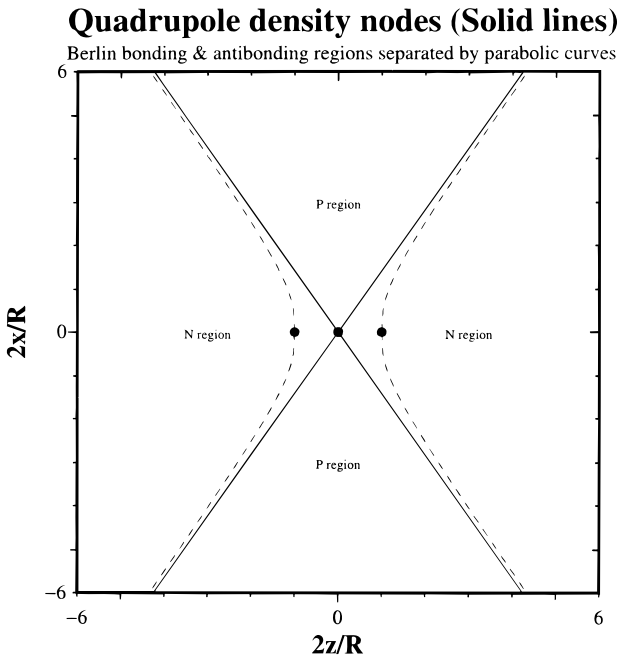

Figure 6. Nodes of $-{}^1/_2(3\cos^2\theta - 1)$ (solid lines) and parabolas separating the Berlin bonding and antibonding regions.

by r^2 (small in this region), and much cancellation results from the integration over $3\cos^2\theta - 1$. The situation with O_2 and F_2 differ only in degree. sp hybridization decreases in going from N_2 to O_2 to F_2, and this is reflected in a less negative value of Θ^{σ}_{mol} in O_2 and F_2, relative to N_2.

The π systems in O_2 and F_2 are qualitatively different from N_2's, and this is reflected in the Θ^{σ}_{mol} curves shown in Figures 3−5. For O_2, δn_π is smaller than in N_2 and, thus, $\Theta^{\pi}_{mol}(O_2)$ is less positive. For F_2, δn_π is almost zero and $\Theta^{\pi}_{mol}(F_2)$ is small. One striking feature of Θ^{π}_{mol} in N_2 and O_2 is the maximum (Figures 3 and 4), which we understand as follows. As the nuclei come together, π electron density accumulates between them (in the P region of Figure 6), and, as R becomes comparable to R_e, some of this density begins to spill over into the N region and thus Θ^{π}_{mol} begins to decrease. The same situation obtains in O_2 and F_2. In O_2, one has less accumulation

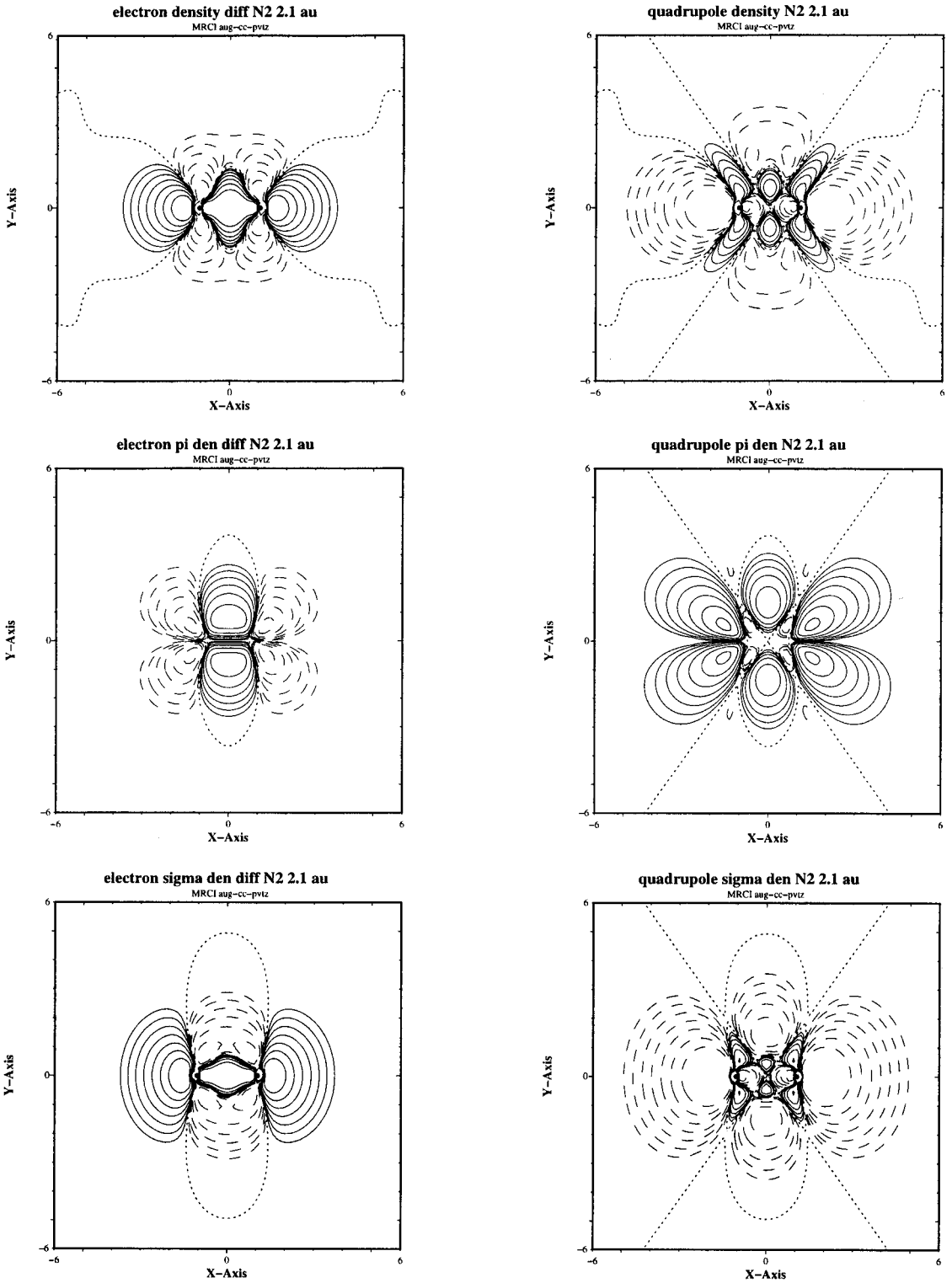

Figure 7. Electron-density difference and the associated quadrupole-density contours for N_2 at $2.1a_0$ calculated with a MRCI wave function and the aug-cc-pvtz basis. The top row shows δn versus $\delta\Theta$; the middle, δn_σ versus $\delta\Theta_\sigma$; the bottom, δn_π versus $\delta\Theta_\pi$. The contour values are $\pm 2^N \times 10^{-3}$ (atomic units) with $N = 0-6$. The dashed contours are negative, the solid contours are positive, and the nodes are dotted. The *x*-axis on the plots is the *z*-axis or internuclear line in the text.

and a smaller increase in $\Theta^{\pi}_{\text{mol}}$, but the same spilling of δn_π into the N region. δn_π for F_2 is rather flat, although one still has a slight maximum in $\Theta^{\pi}_{\text{mol}}$. The equilibrium bond length in these molecules is smaller than the internuclear distance where $\Theta^{\pi}_{\text{mol}}$ is a maximum, so, the slopes of both the π and σ component of Θ are both positive around R_e.

H_2

A similar analysis for H_2 shows that, as the two H atoms approach to form a bond, the density difference δn_σ is positive between the nuclei with a large negative region to the rear of each nucleus. Because of the $3\cos^2\theta - 1$ factor in the quadrupole density integrand, the positive region between the nuclei integrate to a small contribution to $\Theta^{\sigma}_{\text{mol}}$, while the decreased density in the N region of Figure 6 contributes to a large positive $\Theta^{\sigma}_{\text{mol}}$. This characteristic of δn_σ is common to s−s bonds such as H_2, Li_2, Na_2, etc. and opposite to the sp−sp bonds characteristic of N_2, O_2, and F_2. The maximum in $\Theta^{\sigma}_{\text{mol}}$ obtains when large positive components of δn_σ in the N region spill over into the P region, and this happens a little before

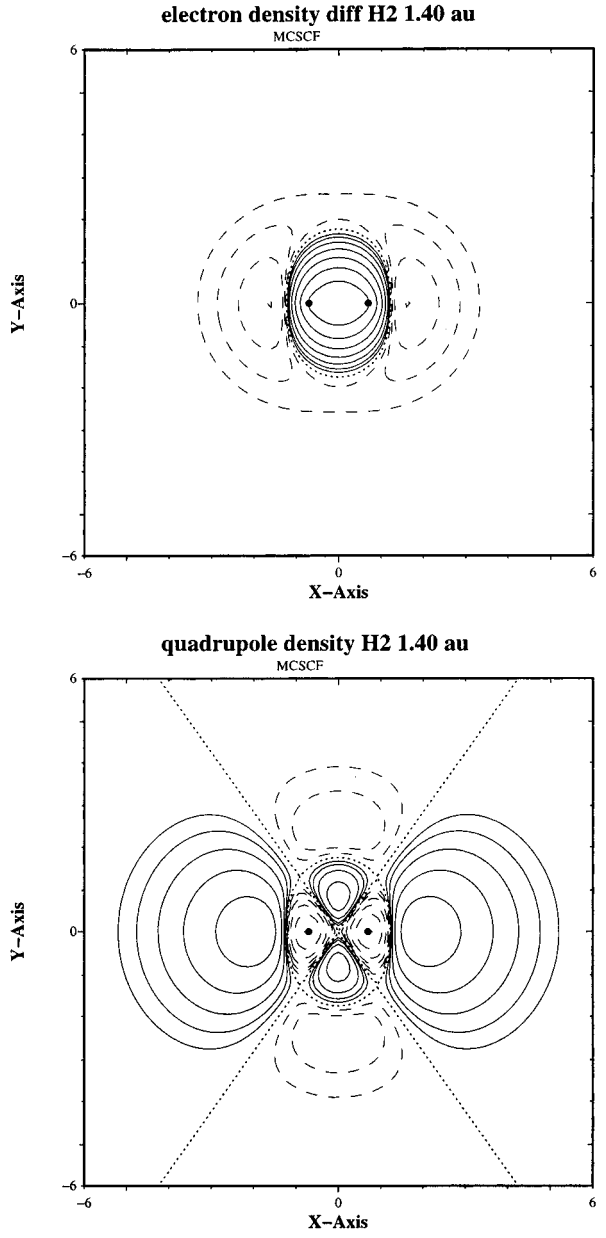

Figure 8. Electron-density difference, δn, and the associated quadrupole-density, $\delta\Theta$, contours for H_2 at $1.4a_0$ calculated with a 10 CSF MCSCF wave function and the aug-cc-pv5z basis. Contour values and conventions are as in Figure 7.

the equilibrium separation. Clearly, Θ will go to zero as $R \rightarrow 0$ and $n(\vec{r};R)$ approaches the united atom limit. These observations are illustrated in Figure 8.

On the Sign of the Molecular Quadrupole Moment

From the preceding discussion, we see that the sign of Θ for N_2, O_2, and F_2 depends on the relative values of Θ_σ (negative) and Θ_π (positive). In F_2, for example, one has a large positive π contribution at ∞, due to the separated atoms, which changes little as the molecule forms because δn_π is small and essentially independent of R. The asymptotically negative σ contribution is reduced further by σ bond formation but not enough to change the sign of Θ, which remains positive. The F_2 σ contribution is anemically negative because of the very slight sp hybridization in F_2. In O_2, the asymptotic value of Θ is less positive than in F_2, and the increased sp hybridization is able to overcome a very positive π contribution and results in a negative quadrupole moment. In N_2, the large sp hybridization causes the Θ_σ to be dominant and Θ is decidedly negative. The situation in H_2 is

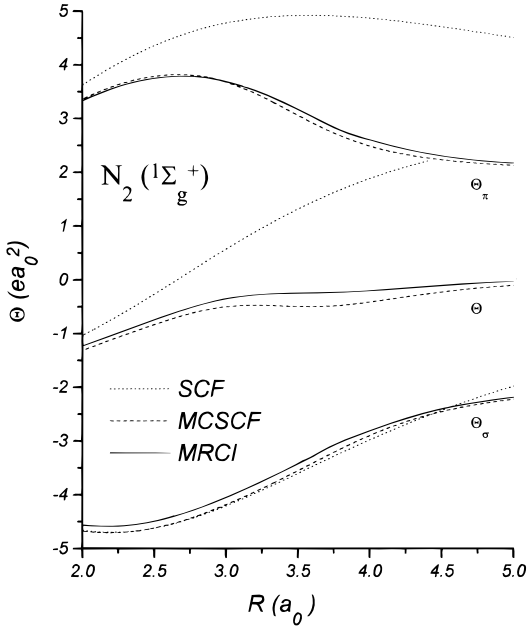

Figure 9. Effect of electron correlation on the magnitude and distance dependence of Θ, Θ_σ, and Θ_π for N_2.

fundamentally different. The sign is always positive because at large R the s−s bond results in δn_σ being negative in the N region, and this situation obtains until the maximum in Θ (H_2;R), after which Θ decreases toward zero, as described above.

Correlation Effects on $\Theta^{\sigma}_{\mathrm{mol}}$ and $\Theta^{\pi}_{\mathrm{mol}}$

Further insight into the relationship between electron correlation and the quadrupole moment obtains from an analysis of Θ_σ and Θ_π. In Figure 9, we plot these quantities for the SCF, MCSCF, and MRCI wave functions of N_2 (aug-cc-pvqz basis). The distance dependence of Θ_σ (around R_e) for all three wave functions is similar, with the SCF and MCSCF contributions being remarkably so. The MRCI value of Θ_σ is the largest of the three and reflects the effect of dynamic correlation in increasing δn_σ in the region between the nuclei. The correlated distance dependence of Θ_π differs markedly from the SCF value and is significantly smaller. These results suggest that the reasonable values of Θ calculated from SCF functions (Table 7) obtain because of a cancellation of errors, Θ_σ(SCF) being too negative and Θ_π(SCF) too positive. Our calculated Θ(SCF) is $-0.9306ea_0^2$, while Θ(CASSCF+1+2) is $-1.1334ea_0^2$, both at $R = 2.07432a_0$. These differ by 18%, and most of the error is in the π contribution.

The corresponding data for O_2 and F_2 are given in Figures 10 and 11. Note that the scales in these plots are identical and the magnitude of the effect of electron correlation on Θ_σ and Θ_π is similar. In O_2, like N_2, Θ_σ (SCF) is too negative, while Θ_π(SCF) is too positive, resulting in a similar cancellation of errors. At $2.28a_0$, we calculate $\Theta(O_2;\mathrm{ROHF}) = -0.2634ea_0^2$ and $\Theta(O_2;\mathrm{CASSCF+1+2}) = -0.2530ea_0^2$, a difference of only 4%, as noted earlier. In F_2, both Θ_σ(SCF) and Θ_π(SCF) are too small, but rather than cancel they add and result in a Θ(SCF) ($0.501ea_0^2$ at $R = 2.68a_0$) compared to the Θ(CASSCF+1+2) value of $0.707ea_0^2$ (a difference of 29%) at the same bond length.

Conclusions

We have studied the quadrupole moments of H_2, N_2, O_2, and F_2 and have estimated the CASSCF+1+2 basis-set limit for the latter three and the CISD limit for H_2. These are in excellent agreement with comparable calculations by others and in good

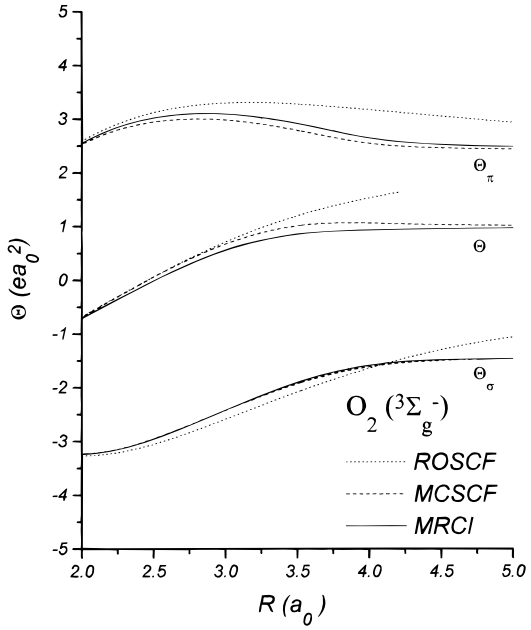

Figure 10. Effect of electron correlation on the magnitude and distance dependence of Θ, Θ_σ, and Θ_π for O_2.

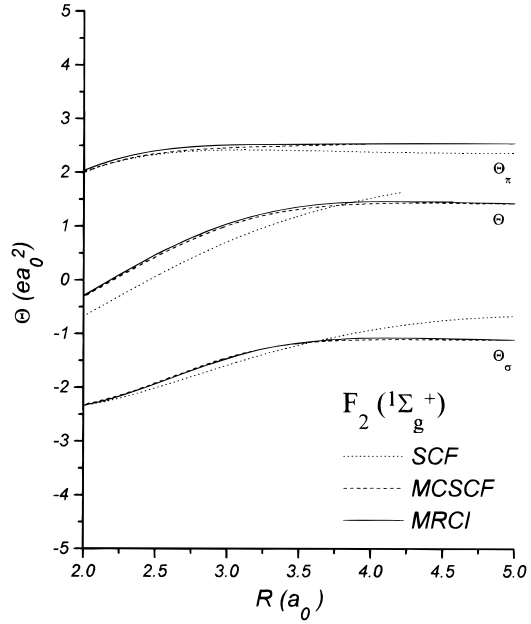

Figure 11. Effect of electron correlation on the magnitude and distance dependence of Θ, Θ_σ, and Θ_π for F_2.

agreement with the existing experimental data. The rather large values of the quadrupole moment derivatives, shown in Table 5, result in the quadrupole moment being a very sensitive function of R around R_{opt}. We have written the global quadrupole-moment function as the sum of an atomic contribution and a molecular contribution Θ_{mol}. The atomic contribution is simply the sum of the quadrupole moments of the constituent (oriented) free atoms, while the molecular contribution is an integral over a quadrupole-density function of the form

$$\delta\Theta = -{}^1/_2(3\cos^2\theta - 1)r^2\,\delta n$$

in which the nuclear contributions are implicit in δn. While not unique, this partitioning of Θ allows us to separate molecular effects from additive atomic effects and provides a deeper understanding of the variation of Θ with R. In particular, the nodal structure of $3\cos^2\theta - 1$ allows us to partition the space in a diatomic molecule into N regions, to the rear of the nuclei and complimentary P regions. Because $\delta\Theta$ is linear in δn, one may define quadrupole densities associated with δn_σ and δn_π and examine the contribution of the σ and π deformation densities to the molecular quadrupole moment. Increases in δn_σ in the N region contribute to make Θ^σ_{mol} negative, while increases in δn_π in the P region make Θ^π_{mol} positive, and, thus, the molecular contribution to the quadrupole moment is the sum of two opposite-signed terms. The total molecular quadrupole moment is the sum of this molecular contribution and the moment due to the sum of the separated atoms. This perspective is useful in understanding the difference in the quadrupole moments of related systems, such as N_2 and P_2, O_2 and S_2, C_6H_6 and C_6F_6, etc.[51] Additionally, the effect of electron correlation on Θ may be partitioned into σ and π contributions via δn_σ and δn_π.

We note that the parabolas that delineate the Berlin bonding and antibonding regions are asymptotically tangent to the nodal surfaces separating the N and P regions (Figure 6). Indeed, the largest contribution to Θ^σ_{mol} and Θ^π_{mol} come from a density difference that is largely localized in the Berlin[47] antibonding and bonding regions, respectively.

Additional details including contour plots and three-dimensional images of δn and $\delta\Theta$, as well as detailed numerical values of Θ as a function of R, have been prepared.[53]

Acknowledgment. This work has been supported, in part, by the MSU Center for Fundamental Materials Research. Several of the Silicon Graphics Workstations used in this work were purchased with an NSF instrument grant, CHE9321436.

References and Notes

(1) (a) Dunning, T. H., Jr. *J. Chem. Phys.* **1989**, *90*, 1007. Kendall, R. A.; Dunning, T. H., Jr.; Harrison, R. J. *J. Chem. Phys.* **1992**, *96*, 6796. Peterson, K. A.; Kendall, R. A.; Dunning, T. H., Jr. *J. Chem. Phys.* **1993**, *99*, 9790. (b) Basis sets were obtained from the Extensible Computational Chemistry Environment Basis Set Database, Version 1.0, as developed and distributed by the Molecular Science Computing Facility, Environmental and Molecular Sciences Laboratory, which is part of the Pacific Northwest Laboratory, P.O. Box 999, Richland, Washington 99352, and funded by the U.S. Department of Energy. The Pacific Northwest Laboratory is a multiprogram laboratory operated by Battelle Memorial Institute for the U.S. Department of Energy under contract DE-AC06-76RLO 1830. Contact David Feller, Karen Schuchardt, or Don Jones for further information.

(2) Frisch, M. J.; Trucks, G. W.; Head-Gordon, M.; Gill, P. M. W.; Wong, M. W.; Foresman, J. B.; Johnson, B. G.; Schlegel, H. B.; Robb, M. A.; Replogle, E. S.; Gomperts, R.; Andres, J. L.; Raghavachari, K.; Binkley, J. S.; Gonzalez, C.; Martin, R. L.; Fox, D. J.; Defrees, D. J.; Baker, J.; Stewart, J. J. P.; Pople, J. A. *Gaussian 92*, Revision A Gaussian, Inc.: Pittsburgh PA, 1992.

(3) Shepard, R.; Shavitt, I.; Pitzer, R. M.; Comeau, D. C.; Pepper, M.; Lischka, H.; Szalay, P. G.; Ahlrichs, R.; Brown, F. B.; Zhao, J. G. *Int. J. Quantum Chem. Symp.* **1988**, *22*, 149.

(4) Buckingham, A. D. *Adv. Chem. Phys.* **1967**, *12*, 107.

(5) Woon, D. E.; Dunning, T. H., Jr. *J. Chem. Phys.* **1993**, *99*, 1914.

(6) Kolos, W.; Wolniewicz, L. *J. Chem. Phys.* **1965**, *43*, 2429.

(7) Stogryn, D. E.; Stogryn, A. P. *Mol. Phys.* **1966**, *11*, 371.

(8) McLean, A. D.; Yoshimini, M. *J. Chem. Phys.* **1966**, *45*, 3676.

(9) Ramsy, N. F. *Molecular Beams*; Oxford University Press: London, 1956.

(10) Buckingham, A. D.; Cordle, J. E. *Mol. Phys.* **1974**, *4*, 1037.

(11) Amos, R. D. *Mol. Phys.* **1980**, *39*, 1.

(12) Huber, K. P.; Herzberg, G. Molecular spectra and molecular structure. *Constants of Diatomic Molecules*; (Van Nostrand-Reinhold: New York, 1979; Vol. 4.

(13) Laaksonen, L.; Pyykkö, P.; Sundholm, D. *Comput. Phys. Rep.* **1986**, *4*, 313.

(14) Wolniewicz, L. *J. Chem. Phys.* **1966**, *45*, 515.

(15) Komasa, J.; Thakkar, A. J. *Mol. Phys.* **1993**, *78*, 1039.

(16) Wolinski, K.; Sadlej, A. J.; Karlström, G. *Mol. Phys.* **1991**, *72*, 425.

(17) Kolos, W.; Roothaan, C. C. J. *Rev. Mod. Phys.* **1960**, *32*, 219.

(18) Dickson, R. M.; Becke, A. D. *J. Phys. Chem.* **1996**, *100*, 16105.

(19) Diercksen, G.; Sadlej, A. J. *Theor. Chim. Acta* **1983**, *63*, 69.

(20) Kolos, W.; Wolniewicz, L. *J. Chem. Phys.* **1964**, *41*, 3674.

(21) Sundholm, D.; Pyykkö, P.; Laaksonen, L. *Mol. Phys.* **1985**, *56*, 1411.

(22) Maroulis, G.; Thakkar, A. J. *J. Phys. B* **1987**, *20*, L551.
(23) McCullough, E. A., Jr. *Mol. Phys.* **1981**, *42*, 943.
(24) Maroulis, G.; Thakkar, A. J. *J. Chem. Phys.* **1988**, *88*, 7623.
(25) Feller, D.; Boyle, C. M.; Davidson, E. R. *J. Chem. Phys.* **1987**, *86*, 3424.
(26) Bündgen, P.; Green, F.; Thakker, A. J. *J. Mol. Struct.* **1995**, *334*, 7.
(27) Laaksonen, L.; Sundholm, D.; Pyykkö, P. *Int. J. Quantum Chem.* **1985**, *xxvii*, 601.
(28) Duffy, P.; Chong, D. P. *J. Chem. Phys.* **1995**, *102*, 3312.
(29) Becke, A. D. *J. Chem. Phys.* **1982**, *76*, 6037.
(30) Piecuch, P.; Kondo, A. E.; Spirko, V.; Paldus, J. *J. Chem. Phys.* **1996**, *104*, 4699.
(31) Dykstra, E. C.; Liu, S.; Malik, D. J. *Adv. Chem. Phys.* **1989**, *75*, 37.
(32) Maroulis, G.; Thakkar, A. J. *J. Chem. Phys.* **1989**, *90*, 366.
(33) Spurling, T. H.; Mason, E. A. *J. Chem. Phys.* **1967**, *46*, 322.
(34) Ely, J. F.; Hanley, H. J. M.; Straty, G. C. *J. Chem. Phys.* **1973**, *59*, 842.
(35) Spirko, V.; Piecuch, P.; Kondo, A.; Paldus, J. *J. Chem. Phys.* **1996**, *104*, 4716.
(36) Buckingham, A. D.; Graham, C.; Williams, J. H. *Mol. Phys.* **1983**, *49*, 703.
(37) Graham, C.; Pierrus, J.; Raab, R. E. *Mol. Phys.* **1989**, *67*, 939.
(38) Truhlar, D. G. *Int. J. Quantum Chem.* **1972**, *VI*, 975.
(39) Maroulis, G.; Bishop, D. M. *Mol. Phys.* **1986**, *58*, 273.
(40) Cartwright, D. C.; Dunning, T. H. *J. Phys. B* **1974**, *7*, 1776.
(41) Buckingham, A. D.; Disch, R. L.; Dummur, D. A. *J. Am. Chem. Soc.* **1968**, *90*, 3104.
(42) Cohen, R. E.; Birnbaum, G. *J. Chem. Phys.* **1977**, *66*, 2443.
(43) Camy Plyret, C.; Flaud, J. M.; Delbouille, L.; Roland, G.; Brault, J. W.; Testerman, L. *J. Phys. Lett.* **1981**, *42*, L279.
(44) Reddy, S. P.; Cho, C. W. *Can. J. Phys.* **1965**, *43*, 2331.
(45) Shapiro, M. M.; Gush, H. P. *Can. J. Phys.* **1966**, *44*, 949.
(46) Reuter, D.; Jennings, D. E. *J. Mol. Spectrosc.* **1986**, *115*, 294.
(47) Birnbaum, G. J.; Cohen, E. R. *Mol. Phys.* **1976**, *32*, 161.
(48) Rijks, W.; van Heeringen, M.; Wormer, P. E. S. *J. Chem. Phys.* **1989**, *90*, 6501.
(49) Wahl. A. C. *J. Chem. Phys.* **1964**, *41*, 2600.
(50) Lawson, D. Ph.D. Thesis, Michigan State University, 1997.
(51) Lawson, D.; Harrison, J. F. To be published.
(52) Berlin, T. *J. Chem. Phys.* **1951**, *19*, 208.
(53) Lawson, D.; Harrison, J. F. Unpublished work. Available via the World Wide Web at: www.cem.msu.edu/∼harrison.